Relaxor ferroelectricity and electric-field-driven structural transformation in the giant lead-free piezoelectric (Ba,Ca)(Ti, Zr)O_3

Kumar Brajesh,[1] Khagesh Tanwar,[2] Mulualem Abebe,[1] and Rajeev Ranjan[1,*]
[1]*Department of Materials Engineering, Indian Institute of Science, Bangalore 560012, India*
[2]*Department of Ceramics Engineering, Indian Institute of Technology, BHU, India*
(Received 10 November 2015; revised manuscript received 30 November 2015; published 23 December 2015)

There is great interest in lead-free $(Ba_{0.85}Ca_{0.15})(Ti_{0.90}Zr_{0.10})O_3$ (15/10BCTZ) because of its exceptionally large piezoelectric response [Liu and Ren, Phys. Rev. Lett. **103**, 257602 (2009)]. In this paper, we have analyzed the nature of: (i) crystallographic phase coexistence at room temperature, (ii) temperature- and field-induced phase transformation to throw light on the atomistic mechanisms associated with the large piezoelectric response of this system. A detailed temperature-dependent dielectric and lattice thermal expansion study proved that the system exhibits a weak dielectric relaxation, characteristic of a relaxor ferroelectric material on the verge of exhibiting a normal ferroelectric-paraelectric transformation. Careful structural analysis revealed that a ferroelectric state at room temperature is composed of three phase coexistences, tetragonal ($P4mm$) + orthorhombic ($Amm2$) + rhombohedral ($R3m$). We also demonstrate that the giant piezoresponse is associated with a significant fraction of the tetragonal phase transforming to rhombohedral. It is argued that the polar nanoregions associated with relaxor ferroelectricity amplify the piezoresponse by providing an additional degree of intrinsic structural inhomogeneity to the system.

DOI: 10.1103/PhysRevB.92.224112 PACS number(s): 77.84.Cg, 77.80.Jk, 61.66.Fn

I. INTRODUCTION

The motivation to replace the commercial high performance piezoelectric lead zirconate titanate (PZT) with a nontoxic substitute has led to a great surge in research interest in lead-free piezoelectrics in the past decade [1–3]. A remarkable breakthrough was the discovery of anomalously high piezoelectric response ($d_{33} \sim 600$ pC/N) in (Ba, Ca)(Ti, Zr)O_3 (generally abbreviated as BCTZ) ceramics [3]. Since then this system has attracted great attention [4–9]. Using phenomenological consideration, Liu and Ren attributed the large piezoresponse to the isotropic flattening of the free-energy profile due to the system's proximity to a cubic-tetragonal-rhombohedral triple point [3]. Based on temperature-dependent dielectric measurements other groups have, however, proposed the existence of an intermediate orthorhombic phase between the rhombohedral and the tetragonal phases and attributed the large piezoelectric response to the orthorhombic phase [7–9]. The proposition of an intermediate orthorhombic phase is in accordance with the sequence of phase transitions exhibited by the parent compound $BaTiO_3$: cubic ($Pm3m$)-tetragonal ($P4mm$) at ∼130 °C, tetragonal ($P4mm$)-orthorhombic ($Amm2$) at ∼0 °C, and orthorhombic ($Amm2$)-rhombohedral ($R3m$) at ∼−90 °C. Substitution of Zr, Sn, and Hf in $BaTiO_3$ brings the three transitions in $BaTiO_3$ close to each other [10–17], eventually making them meet somewhere above the room temperature for compositions in the range of 8–10 mol %. It was recently shown that a mere 2 to 3 mol % of these substitutions could induce a coexistence of tetragonal and orthorhombic phases at room temperature, leading to abrupt enhancement in the piezoelectric response [18–21]. It is intriguing that despite the similarity of the phase diagram of BCTZ [7] and the single element (Zr-, Sn-, or Hf-) modified $BaTiO_3$ systems [10–17], the enhanced piezoelectric response in Zr, Sn, and Hf-modified $BaTiO_3$ is considerably lower ($d_{33} \sim 300-400$ pC/N) than what could be achieved in the BCTZ ($d_{33} \sim 600$ pC/N). This difference can be likened to the difference in the values of the piezoelectric response of the morphotropic phase boundary (MPB) composition of pure PZT ($d_{33} \sim 250-300$ pC/N) and soft (La-modified) PZT ($d_{33} \sim 600$ pC N). From the structural stand point both the pure and the soft PZT exhibit coexistence of ferroelectric phases and field-induced structural transformation [22–24]. These features are consistent with flattening of the free-energy profile and polarization rotation theory [25–28]. The significant difference in the piezoelectric properties of pure PZT and La-modified soft PZT and between Zr-, Sn-, Hf-modified $BaTiO_3$ and BCTZ cannot be understood purely on the basis of the general phenomenological thermodynamic considerations.

La modifications of PZT and $PbTiO_3$ have been reported to break the long-range polar order and induce relaxor ferroelectricity [29–33]. Evidence of polar relaxation has also been reported in a La-modified soft PZT, exhibiting $d_{33} \sim 600$ pC N [24]. These results seem to indicate that the relaxor behavior in soft PZT could be an essential factor and may contribute to the amplification of the piezoelectric response beyond what could be achieved in pure MPB-PZT. In this context, it may be worth mentioning that a very large piezoelectric response is obtained when relaxor ferroelectrics $Pb(Mg_{1/3}Nb_{2/3})O_3$ and $Pb(Zn_{1/3}Nb_{2/3})O_3$ are alloyed with ferroelectric $PbTiO_3$ [34]. Alloying with $PbTiO_3$ gradually decreases the dielectric relaxation and eventually stabilizes an MPB with coexistence of ferroelectric phases [35,36]. The presence of charge, chemical, and structural heterogeneities in relaxor ferroelectrics enhances the polar and elastic susceptibilities of the system [37]. Although no serious attention has so far been given on the possibility of relaxor ferroelectricity in the BCTZ, this possibility cannot be ruled out in view of the fact that a normal to relaxor-ferroelectric crossover happens in Zr-modified $BaTiO_3$ and that this relaxor-ferroelectric system

*rajeev@materials.iisc.ernet.in

has been extensively studied as a model to understand the mechanisms associated with relaxor ferroelectricity [38–46]. Motivated by the possible correlation between the relaxor ferroelectricity and the very large piezoelectric response in soft PZT, $Pb(Mg_{1/3}Nb_{2/3})O_3 - PbTiO_3$ (PMN-PT), and $Pb(Zn_{1/3}Nb_{2/3})O_3 - PbTiO_3$ (PZN-PT) alloys, we probed for such a correlation in the BCTZ system. A detailed dielectric, ferroelectric, piezoelectric, and temperature- and field-dependent high-resolution structural analysis was carried out on 15/10 BCTZ, the composition most reported in literature. We show that deep in the cubic phase region (~100 °C above the dielectric anomaly temperature) the system exhibits: (i) the onset of spontaneous electrostrictive strain, (ii) dielectric dispersion, and (iii) a departure from Curie-Weiss behavior below a characteristic Burn's temperature. These features are quintessential of a relaxor ferroelectric thereby proving that the ferroelectric state observed at room temperature is a result of spontaneous relaxor to normal ferroelectric transformation and not due to phase transformation in the thermodynamic sense as is generally anticipated for MPB systems. We show that the ferroelectric state at room temperature is characterized by the coexistence of three ferroelectric phases, tetragonal ($P4mm$), orthorhombic ($Amm2$), and rhombohedral ($R3m$). The giant piezoresponse is also shown to be associated with a significant fraction of the tetragonal phase transforming to rhombohedral on application of an electric field. Our results suggest that the twin occurrence of relaxor ferroelectricity and field-induced transformation is responsible for the very large piezoelectric response in this system.

II. EXPERIMENT

$(Ba_{0.85}Ca_{0.15})(Ti_{0.90}Zr_{0.10})O_3$ (15/10 BCZT) was prepared via a conventional solid-state route. High-purity $BaCO_3$ (99.8%; Alfa Aesar), $CaCO_3$ (99.99%; Alfa Aesar), TiO_2 (99.8%; Alfa Aesar), and ZrO_2 were wet milled in a zirconia jar with zirconia balls as the mixing media and acetone as the wetting agent for 12 h using a planetary ball mill (Fritsch P5). The thoroughly mixed powder was calcined at 1300 °C for 4 h and milled again in acetone for 5 h for better homogenization. The calcined powder was mixed with 2 wt % polyvinyl alcohol and pressed into disks of 15-mm diameter by using uniaxial dry pressing at 10 ton. Sintering of the pellets was carried out at 1550 °C for 2 h under ambient conditions. X-ray powder diffraction was performed using a Rigaku (SMART LAB) diffractometer with a Johanson monochromator in the incident beam to remove the Cu $K\alpha_2$ radiation. A dielectric measurement was carried out using a Novocontrol (Alpha AN) impedance analyzer. Measurement of the longitudinal piezoelectric coefficient (d_{33}) was carried out using piezotest PM 300 by poling the pellets at room temperature for 1 h at a field of ~2.2 kV/mm. The strain loop and the polarization electric-field hysteresis loop were measured with a Precision premier II loop tracer. Structure refinement was carried out using FULLPROF software [47].

III. RESULTS

A. Dielectric and piezoelectric study

The poled specimen of 15/10 BCZT exhibited a longitudinal piezoelectric coefficient (d_{33}) of ~570 pC N as measured by a commercial Berlincourt based piezometer (Piezotest PM 300). This value is comparable to that reported by Liu and Ren [3]. Figure 1 shows the polarization and electric-field-induced bipolar strain. The polarization-electric-field loop exhibits a well-defined hysteresis with a remanence of ~23.72 $\mu C\,cm^2$. The specimen showed a large piezostrain of ~0.27% at an electric field of 40 kV cm as shown in the inset of Fig. 1. This value is nearly three times the value observed for pure $BaTiO_3$ (~0.1%) and is even larger than the value (~0.19%) reported earlier [21]. The large value of the high-field piezostrain as well as the weak-field direct d_{33} suggests that this specimen is a good candidate for actuator and sensor applications.

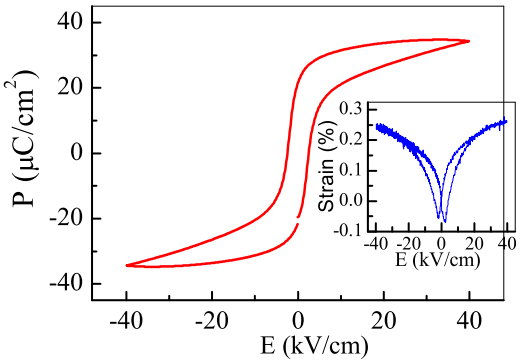

FIG. 1. (Color online) Electric-field dependence polarization and strain (in the inset).

B. Evidence of the coexistence of ferroelectric phases at room temperature

Figure 2 shows a comparison of the x-ray powder diffraction (XRPD) profiles of pseudocubic $\{111\}_{pc}$, $\{200\}_{pc}$, $\{222\}_{pc}$, and

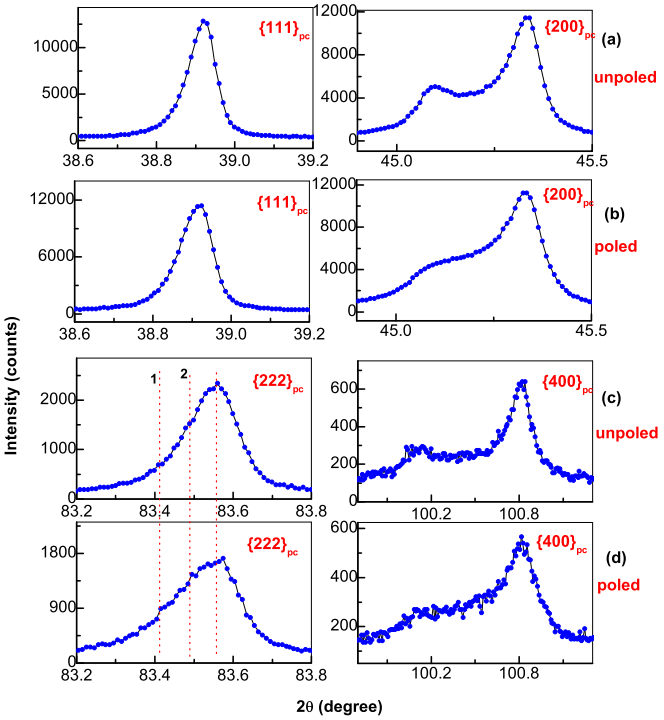

FIG. 2. (Color online) Pseudocubic $\{111\}_{pc}$, $\{200\}_{pc}$, $\{222\}_{pc}$, and $\{400\}_{pc}$ XRD profiles of unpoled and poled 15/10 BCTZ.

$\{400\}_{pc}$ of unpoled and poled specimens. The XRD pattern of the poled specimen was obtained by grinding the poled pellet to powder. This way one can avoid preferred orientation effects in the diffraction pattern and obtain accurate first-hand information with regard to the nature of the field-induced structural transformation, if any, by analyzing the difference in the patterns of the unpoled and the poled specimens. The success of this strategy has been demonstrated before in different piezoelectric systems [21,24,48–50]. A first glance at Fig. 2(a) suggests the singlet nature of $\{111\}_{pc}$ and the doublet nature of $\{200\}_{pc}$, implying a tetragonal ($P4mm$) global structure. The profiles appear to be broadened for the poled specimen, Fig. 2(b). More detailed information was, however, obtained from careful analysis of the higher-order reflections $\{222\}_{pc}$ and $\{400\}_{pc}$, Figs. 2(c) and 2(d). The $\{222\}_{pc}$ profile of the poled specimen develops distinct humps, one at $2\theta = 83.4^{\circ}$ (labeled 1) and another at $2\theta = 83.48^{\circ}$ (labeled 2). For the sake of direct comparison with the $\{222\}_{pc}$ profile of the unpoled specimen, a vertical dashed line is drawn at both positions. This helped in identifying the existence of similar humps, although with a weaker intensity, in the unpoled specimen. We would like to emphasize that without such a comparison, it would be difficult to suggest additional features in the unpoled pattern, as such weak humps are generally ignored. The two additional humps in $\{222\}_{pc}$ unambiguously confirm the presence of other phase(s) in addition to the tetragonal phase in both the unpoled and the poled specimens. Their enhanced intensity in the pattern of the poled specimen suggests that the poling field has increased the volume fraction of the additional phases. The nature of the additional phases and the effect of the poling field on their relative fractions is discussed in the next section.

C. The nature of phase coexistence

To ascertain the nature of the additional phase(s) in 15/10 BCTZ, a detailed fitting of the XRPD pattern was carried out using different combinations of phases by the Rietveld method. For the sake of clarity and direct comparison of the fits obtained with different structural models, we show the fits of the high angle profiles in Fig. 3 (for the poled specimen) and Fig. 4 (for the unpoled specimen). For reference, we also carried out a fit with single phase $P4mm$. Evidently, the fit turned out to be highly unsatisfactory. Since the additional peaks are more prominent in the poled pattern, we first focused our attention on the analysis of the poled pattern. First, we considered two different two-phase models $P4mm + R3m$ and $P4mm + Amm2$. The fits shown in Figs. 3(b), 3(c), 4(b), and 4(c) suggest that both two-phase models cannot account for the all the profiles satisfactorily. In the next step we considered all three phases $P4mm + Amm2 + R3m$ together. This resulted in satisfactory fits of both the poled and the unpoled patterns [Figs. 3(d) and 4(d)]. From the best fit obtained with the three-phase model, it became clear that the additional peaks in the $\{222\}_{pc}$ profile at 83.41° and 83.48° (labeled 1 and 2) are characteristic of the $R3m$ and

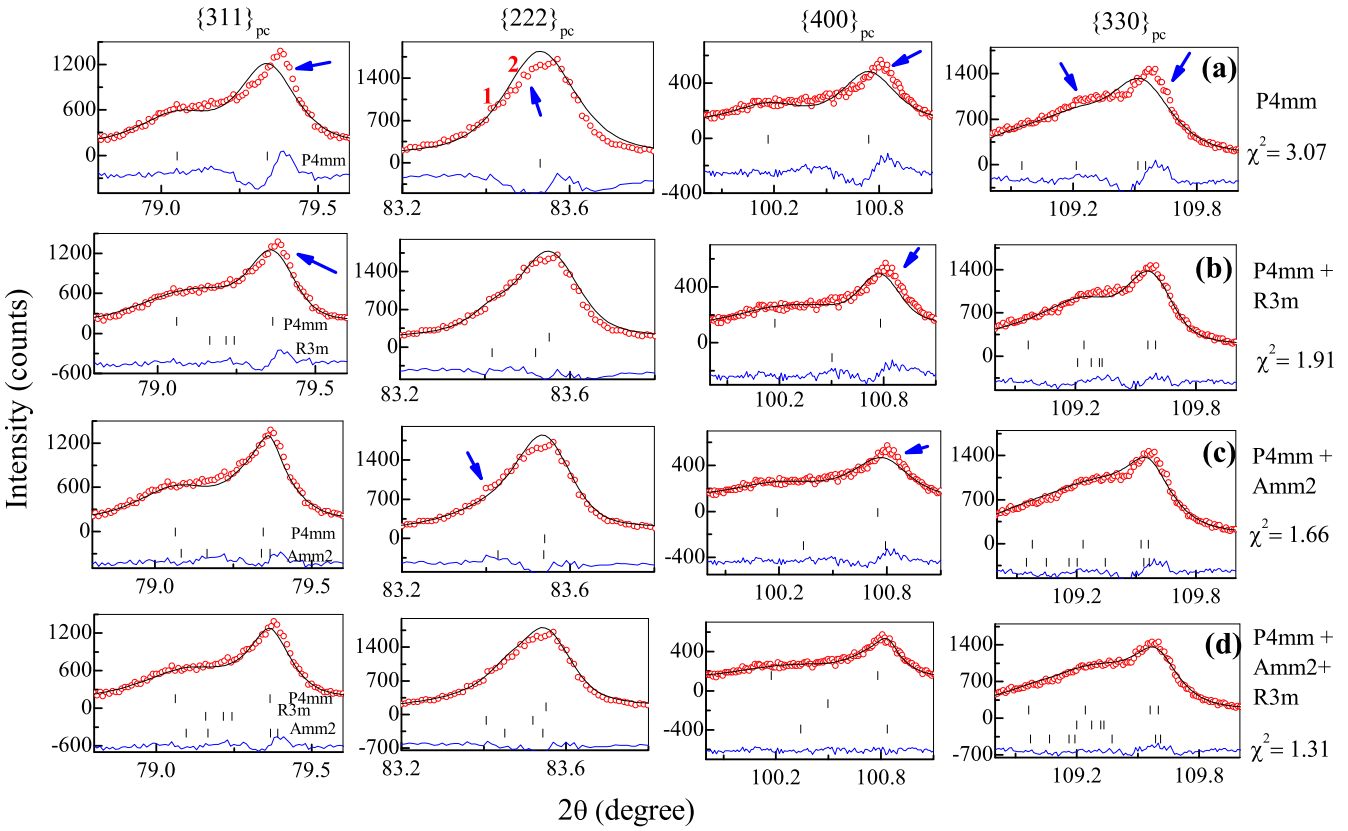

FIG. 3. (Color online) Rietveld fitted x-ray powder diffraction patterns of poled 15/10 BCTZ with (a) $P4mm$, (b) $P4mm + R3m$, (c) $P4mm + Amm2$, and (d) $P4mm + Amm2 + R3m$ models. The arrows highlight the misfit regions. The numbers 1 and 2 are the labels of the additional peaks in the $\{222\}_{pc}$ profile, also specified in Fig. 2.

TABLE I. Refined structural parameters and agreement factors for the unpoled $(Ba_{0.85}Ca_{0.15})(Ti_{0.9}Zr_{0.1})O_3$ using the tetragonal ($P4mm$) + orthorhombic ($Amm2$) + rhombohedral ($R3m$) phase coexistence model.

Space group: $P4mm$					Space group: $Amm2$				Space group: $R3m$			
Atoms	x	Y	Z	B(Å^2)	x	y	z	B(Å^2)	x	y	z	B(Å^2)
Ba/Ca	0.000	0.000	0.000	0.12(3)	0.00	0.000	0.000	0.35(2)	0.000	0.000	0.000	0.12(4)
Ti/Zr	0.500	0.500	0.508(3)	0.15(3)	0.500	0.000	0.497(4)	0.41(3)	0.000	0.000	0.5226	0.19(5)
O1	0.500	0.500	−0.001(2)	0.11(6)	0.000	0.000	0.544(4)	0.16(8)	0.312(0)	0.18(0)	0.66(2)	0.47(8)
O_2	0.500	0.000	0.508(8)	0.10(8)	0.500	0.255(2)	0.24(1)	0.48(9)				
$a = 3.9986(4)$ Å, $c = 4.0192(5)$Å, $v = 64.265(1)$ Å^3, and % phase = 56.21(3)					$a = 3.9996(1)$ Å, $b = 5.6759(2)$ Å, $c = 5.6648(2)$Å, $v = 128.602\,(6)$ Å^3, and % phase = 31.77(2)				$a = 5.6736(8)$ Å, $c = 6.9309(3)$ Å, $v = 193.217(5)$ Å^3, and % phase = 12.02(2)			
R_p : 10.8, R_{wp} : 11.5, R_{exp} : 9.57, χ^2: 1.48												

TABLE II. Refined structural parameters and agreement factors for the poled $(Ba_{0.85}Ca_{0.15})(Ti_{0.9}Zr_{0.1})O_3$ using tetragonal ($P4mm$) + orthorhombic ($Amm2$) + rhombohedral ($R3m$) phase coexistence model.

Space group: $P4mm$					Space group: $Amm2$				Space group: $R3m$			
Atoms	x	Y	Z	B(Å^2)	x	y	z	B(Å^2)	x	y	z	B(Å^2)
Ba/Ca	0.000	0.000	0.000	0.28(3)	0.00	0.000	0.000	0.13(4)	0.000	0.000	0.000	0.78(7)
Ti/Zr	0.500	0.500	0.480(3)	0.15(5)	0.500	0.000	0.483(4)	0.38(3)	0.000	0.000	0.498(7)	0.52(6)
O_1	0.500	0.500	0.01(2)	0.32(1)	0.000	0.000	0.579(8)	0.33(8)	0.312	0.18	0.641(1)	0.38(8)
O_2	0.500	0.000	0.48(2)	0.48(1)	0.500	0.2550	0.27(2)	0.25(9)				
$a = 3.9992(5)$ Å, $c = 4.0169(4)$ Å, $v = 64.248(2)$ Å^3, and % phase = 37.16(2)					$a = 3.9976(2)$ Å, $b = 5.6777(4)$Å, $c = 5.6701(1)$ Å, $v = 128.698\,(6)$ Å^3, and % phase = 33.97(2)				$a = 5.6651(3)$ Å, $c = 6.9469(1)$ Å, $v = 193.081(3)$ Å^3, and % phase = 28.87(4)			
R_p : 10.8, R_{wp} : 11.57, R_{exp} : 9.5, χ^2: 1.31												

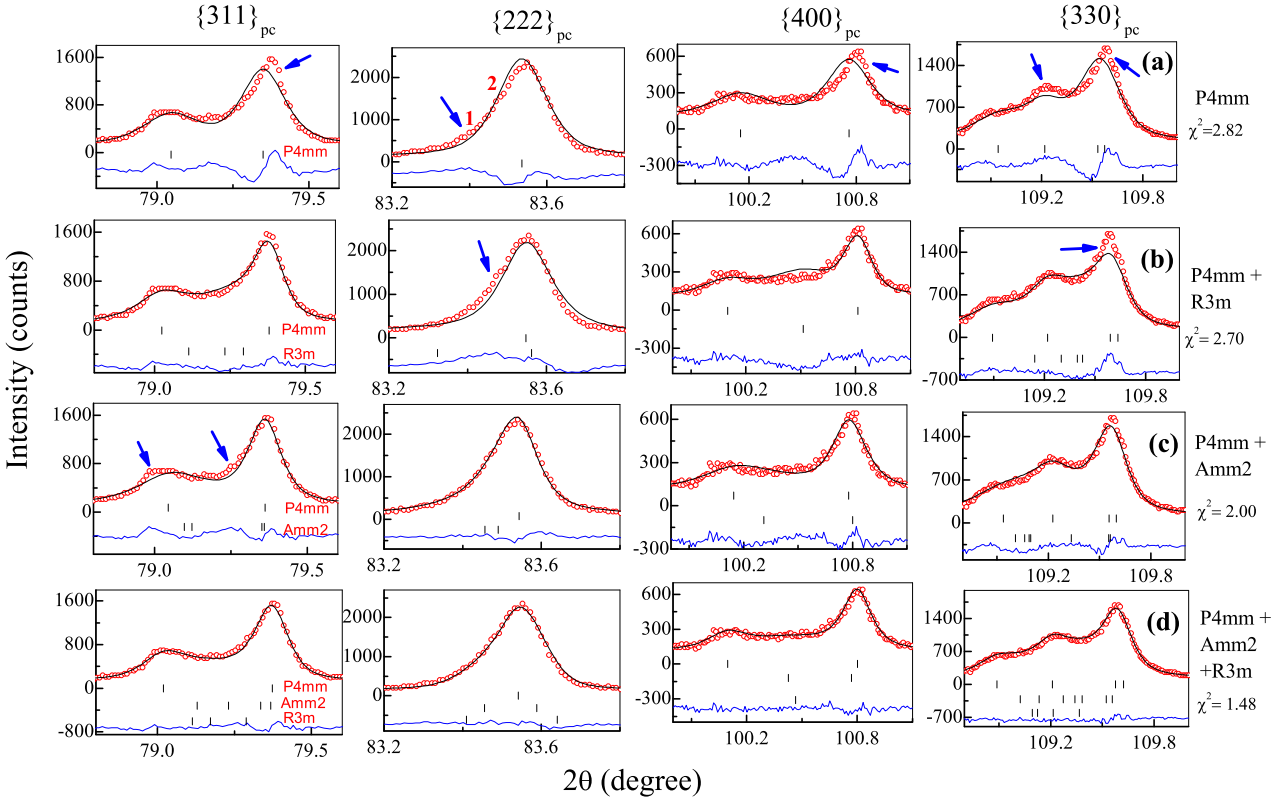

FIG. 4. (Color online) Rietveld fitted x-ray powder diffraction patterns of unpoled 15/10 BCTZ with (a) $P4mm$, (b) $P4mm + R3m$, (c) $P4mm + Amm2$, and (d) $P4mm + Amm2 + R3m$ models. The arrows highlight the misfit regions.

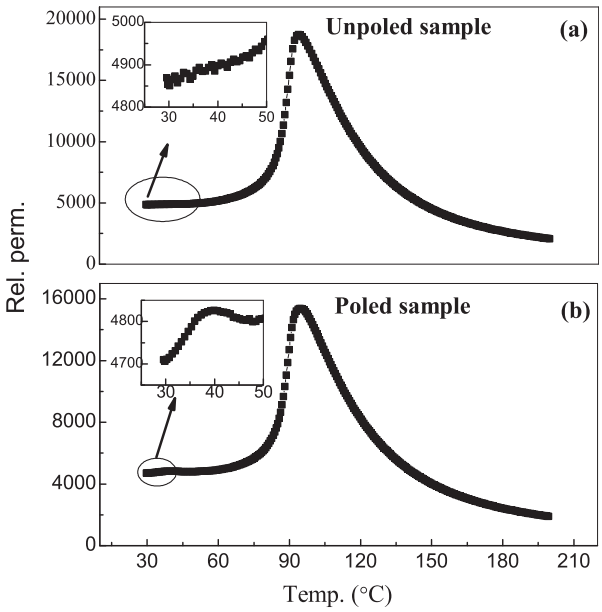

FIG. 5. Temperature dependence of the relative permittivity at 1 kHz of (a) unpoled and (b) poled 15/10 BCTZ.

*Amm*2 phases, respectively. The refined structural parameters of the unpoled and the poled specimens are given in Tables I and II. The most important difference between the poled and the unpoled specimens is in the relative volume fractions of the three coexisting phases. The tetragonal fraction decreased from 56% to 37%, i.e., by 19% after poling. The *Amm*2 and the *R*3*m* fractions increased by 3% and 16%, respectively. This proves that the electric field transformed the *P*4*mm* phase to *R*3*m* + *Amm*2 at room temperature. The increased volume fraction of the *R*3*m* and *Amm*2 phases after poling also influenced the permittivity-temperature curve—the poled specimen exhibits a weak dielectric anomaly at ∼40 °C which was not found in the unpoled specimen, Fig. 5.

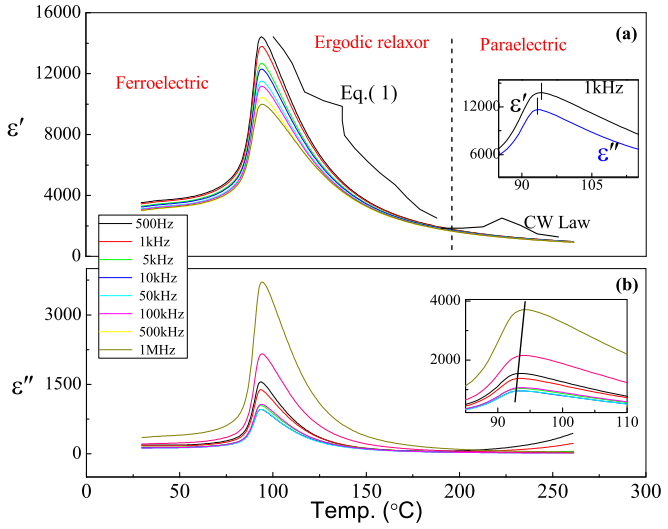

FIG. 6. (Color online) Temperature variation of (a) real and (b) imaginary parts of relative permittivity at different frequencies of 15/10 BCTZ. The inset in (a) shows a magnified plot of real and imaginary parts on a magnified scale to reveal that the imaginary pert peaks at a slightly lower temperature than the corresponding real part at a given frequency (1 kHz). The inset in (b) shows a magnified plot of the imaginary part to reveal the frequency dependence of the peak temperature.

D. Evidence of an ergodic relaxor state

Figure 6(a) shows the temperature dependence of the relative permittivity of 15/10 BCTZ at several frequencies. A considerable dispersion can be seen near the dielectric anomaly temperature (∼94 °C). The degree of dispersion decreases with increasing temperature and vanishes above ∼200 °C, thereby suggesting that it owes its origin to the formation of polar nanoregions [51,52], a phenomenon which is typical of relaxor ferroelectrics. We also noted other characteristic features of relaxor ferroelectricity, such as the peaking of the imaginary part at a lower temperature than the real part [the inset of Fig. 6(a)] and shifting of the permittivity peaks to a higher temperature with increasing frequency [the inset of Fig. 6(b)]. A significant departure from the Curie-Weiss behavior was also found below 200 °C, Fig. 7(a). Additional confirmation of the relaxor behavior was found in the lattice thermal expansion study. As shown in Fig. 7(b), a noticeable

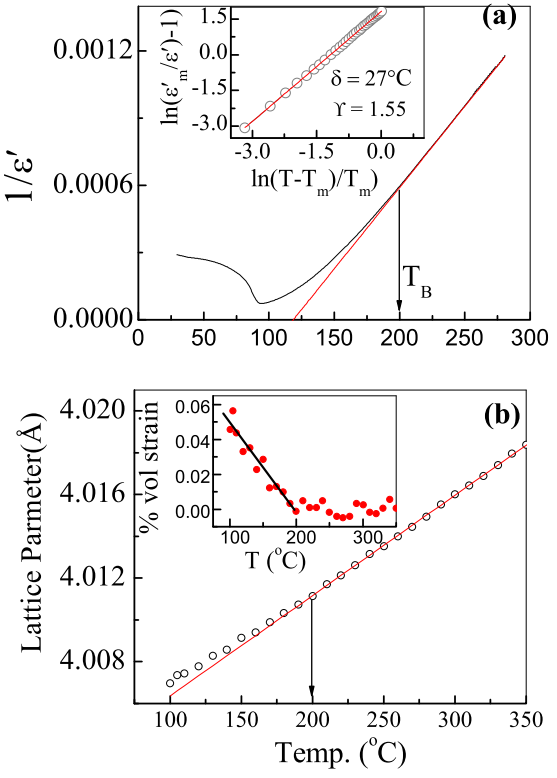

FIG. 7. (Color online) (a) Curie-Weiss fit of the real part of the permittivity data of 15/10 BCTZ. T_B corresponds to Burn's temperature. The inset shows the fitting of Eq. (1) in the text to derive the degree of diffuseness (δ) of the permittivity peak and the deviation parameter (γ) from the Curie-Weiss law. (b) shows the variation of cubic lattice parameter with temperature. The continuous line is the best linear fit above Burn's temperature. The inset in (b) shows percentage electrostrictive volume strain as a function of temperature below Burn's temperature.

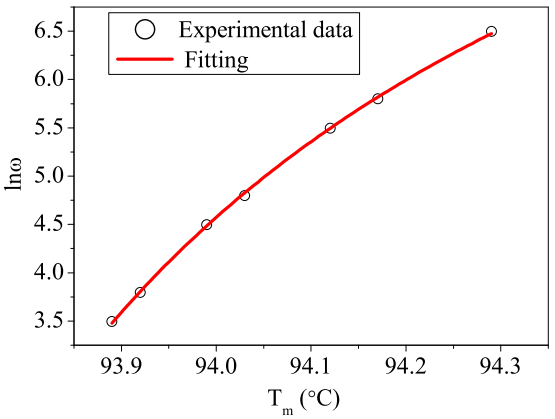

FIG. 8. (Color online) Vogel-Fulcher fit to the permittivity peak temperature as a function of frequency.

departure from linear thermal expansion behavior sets in below 200 °C, the temperature below which dielectric dispersion as well as a departure from Curie-Weiss behavior also sets in. The excess value of the cubic cell volume below 200 °C, shown in the inset of Fig. 7(b), is due to the spontaneous electrostrictive strain associated with the formation of dynamic polar nanoregions. The 200 °C can therefore be identified as the Burn's temperature of this system. These results confirm the occurrence of relaxor ferroelectricity in 15/10 BCTZ. Following Bokov *et al.* [51] and Bokov and Ye [52], the diffuseness (δ) of the permittivity peak and departure from the Curie-Weiss behavior (γ) in relaxor ferroelectrics was parametrized by fitting the permittivity in the temperature range of 95–200 °C using a generalized expression,

$$(\varepsilon_m/\varepsilon) = 1 + (T - T_m)^{\gamma}/2\delta^2. \quad (1)$$

The fit is shown in the inset of Fig. 7(a) with $\gamma = 1.55$ and $\delta = 27\,^{\circ}\mathrm{C}$.

Further verification of the relaxor behavior was carried out by fitting the Vogel-Fulcher [33,35] empirical relation,

$$\omega = \omega_0 \exp\left[\frac{-E_a}{K(T_m - T_f)}\right] \quad (2)$$

to the frequency dependence of the dielectric permittivity maximum, Fig. 8. The best fit was obtained with a preexponential factor of 1.5×10^{11} Hz and freezing temperature of $T_f = 92\,^{\circ}\mathrm{C}$, which is just below the dielectric anomaly temperature (~94 °C).

IV. DISCUSSION

The mechanisms related to the large piezoelectric response in ferroelectrics have been extensively discussed in the literature. First-principles and phenomenological studies lay emphasis on the anisotropic flattening of the free-energy profile, allowing polarization rotation along low-energy pathways as the fundamental mechanism [25–27]. The occurrences of field-induced phase transformation have been argued in justification of this mechanism [21,23,24,49,53,54]. Domain walls also contribute to the high piezoelectric response [25,55–57]. Gao *et al.* have reported miniaturization of the tetragonal and rhombohedral domains in BCTZ in the MPB region [58]. It is argued that the miniaturized domains enable easy rotation of polarization and enhance the piezoelectric response. Recently, Hinterstein *et al.* reported that the major contributing mechanism to the overall measured piezostrain in a soft PZT is field-induced phase transformation [59]. In another piezoelectric system $PbTiO_3 - BiScO_3$, Lalitha *et al.* have shown that the domain switching propensity is rather reduced in the MPB composition and attributed the field-induced phase transformation as the dominant contributing mechanism with regard to the large piezoresponse [59]. The high piezoelectric response was accordingly attributed to the field-induced phase transformation [60]. Tian and co-workers proposed that the large piezoelectric response is facilitated in 15/10 BCTZ by an intermediate orthorhombic phase [7,8]. In this description, the orthorhombic (*Amm*2) phase is given the same status as the monoclinic *Cm* phase in PZT [28]. This analogy does not seem to be appropriate since the polarization direction in the *Amm*2 phase is fixed along [110], whereas the *Cm* allows for the continuous rotation of the polarization vector. The three-phase coexistence shown in the present paper may not be unique to 15/10 BCTZ. The fact that the $P4mm - Amm2$ and $Amm2 - R3m$ boundaries of $BaTiO_3$ tend to meet with increasing concentration of Zr, Sn, and Hf, suggests such a possibility, even in the simple systems, $Ba(Ti, Zr)O_3$, $Ba(Ti, Sn)O_3$, and $Ba(Ti, Hf)O_3$. The large piezoelectric response in this system was, however reported for the composition at the tetragonal-orthorhombic boundary and not where the three phases are likely to coexist [18,19,21]. Coexistence of three ferroelectric phases $P4mm + Cm + R3m$ has also been reported for the MPB composition of PZT by Zhang *et al.* [61]. In principle, one can fit the diffraction data of 15/10 BCTZ equally well by considering the $P4mm + Cm + R3m$ model since the structure and lattice parameters of the lower-symmetry *Cm* phase are very similar to that of the *Amm*2 phase. However, we did not feel such a necessity during the refinement as the *Amm*2 along with the *P*4*mm* and *R*3*m* phases were able to account for all the features in the pattern. Furthermore, it is important to bear in mind that in contrast to the existence of a well-defined $Amm2 - R3m$ phase boundary in the $BaTiO_3$-based piezoelectrics, there is no analogous distinct $Cm - R3m$ boundary in PZT. The justification of the *Cm* phase in PZT has been rationalized since the additional parameters it provides (because of its lower symmetry as compared to *R*3*m*) helps in better fitting of the broad peaks of the rhombohedral-like diffraction patterns [62]. The broadening of the peaks in PZT is, perhaps, also associated with the short-range correlation of the Pb displacements [63–65]. The short-range correlation between Pb atoms arises as a result of local repulsive interactions, which is sensitive to the distribution of the Zr/Ti cations [66]. Glazer *et al.* [67] and Zhang *et al.* [68] have argued that the degree of the ordering of such short-ranged clusters determines the average global structures in PZT. The very fact that two very closely spaced peaks, characteristic of *R*3*m* and *Amm*2 phases, could be seen in the pattern of 15/10 BCTZ, suggest that Ba/Ca is not as disordered in 15/10 BCTZ as Pb is in the Pb-based piezoelectrics. Thus, in contrast to Pb-based ferroelectrics, wherein the Pb disorder has a significant influence in enhancing the piezoelectric properties

[67–69], the role of Ba/Ca in 15/10 BCTZ is expected to be limited. The predominant atomistic mechanism which determines polarization and piezoelectricity in 15/10 BCTZ would involve dipoles associated with Ti displacements. Our results suggest that in 15/10 BCTZ the electric field switches Ti displacement from [001] to [111] and [110] directions. The large (16%) increase in the volume fraction of the *R*3*m* phase suggests that the switching propensity is more from the [001] to the [111] direction as compared to the [001] to the [110] direction. As reported by Hinterstein *et al.* [59], although field-induced transformation is likely to be the dominant mechanism for giving rise to the large piezostrain (∼0.3%, Fig. 1) in 15/10 BCTZ, our results suggest that relaxor ferroelectricity also has a role to play in enhancing the piezoelectric response. Compared to the case in conventional relaxor ferroelectrics, such as PMN and PZN [36,37], the dielectric relaxation in the present system is relatively weak. The dielectric behavior of the present system is rather analogous to that of PMN-PT and PZN-PT alloys close to their respective MPBs [35,36]. Xu *et al.* have shown that the polar nanoregions survive even in the nonergodic ferroelectric state of relaxor ferroelectrics [70]. Petzelt and co-workers [44,45] and Nuzhnyy *et al.* [71] have reported that the Ti^{4+} dynamics does not freeze completely in the nonergodic state of $Ba(Ti_{1-x}Zr_x)O_3$. Detailed first-principles-based computational studies have shown that the relaxor state in BZT is caused by the difference in the ferroelectric strengths of the Ti^{4+} and Zr^{4+} ions [46,72,73]. This difference in the off-centering of Zr and Ti ions gives rise to Fano resonance and thermally activated terahertz relaxation. The embedded polar nanoregions in the nonergodic (MPB) ferroelectric state may act as active centers, which, via a synergistic interaction, amplifies the piezoelectric response contribution due to field-induced phase transformation and domain-wall motion.

V. CONCLUSION

In conclusion, we show that the high performance lead-free piezoelectric 15/10 BCTZ exhibits relaxor ferroelectricity, coexistence of three ferroelectric phases, and field-induced phase transformation. The system shows the onset of spontaneous electrostrictive lattice strain, dielectric dispersion, and deviation from Curie-Weiss behavior, below a characteristic Burn's temperature, deep inside the cubic-paraelectric regime, thereby confirming the occurrence of polar nanoregions. These results suggest that the ferroelectric state in this giant piezoelectric system appears as a result of relaxor to normal ferroelectric transformation. Careful structural analysis of the room-temperature ferroelectric state revealed a coexistence of three ferroelectric phases, tetragonal, orthorhombic, and rhombohedral. We also show that the giant piezoresponse is associated with electric-field-induced tetragonal to orthorhombic + rhombohedral transformation. It is argued that the polar nanoregions associated with the relaxor ferroelectricity help in amplifying the piezoelectric response by providing additional degrees of local structural heterogeneity to the system.

ACKNOWLEDGMENT

R.R. acknowledges the Science and Engineering Board (SERB) of the Department of Science and Technology, Government of India (Grant No. SERB/F/5046/2013-14) and ISRO-IISc, Space Technology Cell for financial assistance.

[1] Y. Saito, H. Takao, T. Tani, T. Nonoyama, K. Takatori, T. Homma, T. Nagaya, and M. Nakamura, Nature (London) **432**, 84 (2004).
[2] J. Rödel, W. Jo, K. T. P. Seifert, E.-M. Anton, T. Granzow, and D. Damjanovic, J. Am. Ceram. Soc. **92**, 1153 (2009).
[3] W. Liu and X. Ren, Phys. Rev. Lett. **103**, 257602 (2009).
[4] D. Damjanovic, A. Biancoli, L. Batooli, A. Vahabzadeh, and J. Trodahl, Appl. Phys. Lett. **100**, 192907 (2012).
[5] A. Bjornetun, J. S. Forrester, D. Damjanovic, B. Li, K. J. Bowman, and J. L. Jones, J. Appl. Phys. **113**, 014103 (2013).
[6] D. S. Keeble, F. Benabdallah, P. A. Thomas, M. Maglione, and J. Kreisel, Appl. Phys. Lett. **102**, 092903 (2013).
[7] Y. Tian, L. Wei, X. Chao, Z. Liu, and Z. Yang, J. Am. Ceram. Soc. **96**, 496 (2013).
[8] Y. Tian, X. Chao, L. Jin, L. Wei, P. Liang, and Z. Yang, Appl. Phys. Lett. **104**, 112901 (2014).
[9] Y. Zhang, J. Glaum, C. Groh, M. C. Matthias, J. E. Blendell, K. J. Bowman, and M. J. Hoffman, J. Am. Ceram. Soc. **97**, 2885 (2014).
[10] G. H. Jonker and W. Kwestroo, J. Am. Ceram. Soc. **41**, 390 (1958).
[11] T. N. Verbitskaya, G. S. Zhdanov, Y. N. Venevtsev, and S. P. Solov'ev, Kristallografiya **3**, 186 (1958).
[12] Z. Yu, C. Ang, R. Guo, and A. S. Bhalla, J. Appl. Phys. **92**, 1489 (2002).
[13] N. Yasuda, H. Ohwa, and S. Asano, Jpn. J. Appl. Phys., Pt. 1 **35**, 5099 (1996).
[14] G. H. Jonker, Philips Tech. Rev. **17**, 129 (1955).
[15] G. A. Smolenskii and V. A. Isupov, Dokl. Akad. Nauk SSSR **96**, 53 (1954).
[16] E. G. Fesenko and O. I. Prokopalo, Soviet Phys. Crystallogr. **6**, 373 (1961).
[17] T. N. Verbitskaya, E. I. Gindin, and V. G. Prokhvatilov, Fiz. Tverd. Tela **1**, 180 (1959).
[18] A. K. Kalyani, A. Senyshyn, and R. Ranjan, J. Appl. Phys. **114**, 014102 (2013).
[19] A. K. Kalyani and R. Ranjan, J. Phys.: Condens. Matter **25**, 362203 (2013).
[20] A. K. Kalyani, K. Brajesh, A. Senyshyn, and R. Ranjan, Appl. Phys. Lett. **104**, 252906 (2014).
[21] A. K. Kalyani, H. Krishnan, A. Sen, A. Senyshyn, and R. Ranjan, Phys. Rev. B **91**, 024101 (2015).
[22] K. A. Schnoau, M. Knapp, H. Kungl, M. J. Hoffmann, and H. Fuess, Phys. Rev. B **76**, 144112 (2007).
[23] M. Hinterstein, J. Rouquette, J. Haines, P. Papet, M. Knapp, J. Glaum, and H. Fuess, Phys. Rev. Lett. **107**, 077602 (2011).
[24] A. K. Kalyani, K. V. Lalitha, A. R. James, A. N. Fitch, and R. Ranjan, J. Phys.: Condens. Matter **27**, 072201 (2015).
[25] D. Damjanovic, J. Am. Ceram. Soc. **88**, 2663 (2005).
[26] H. Fu and R. E. Cohen, Nature (London) **403**, 281 (2000).

[27] D. Vanderbilt and M. H. Cohen, Phys. Rev. B **63**, 094108 (2001).
[28] R. Guo, L. E. Cross, S.-E. Park, B. Noheda, D. E. Cox, and G. Shirane, Phys. Rev. Lett. **84**, 5423 (2000).
[29] X. H. Dai, Z. Xu, and D. Viehland, Philos. Mag. B **70**, 33 (1994).
[30] D. Viehland, J. F. Li, S. J. Jang, L. E. Cross, and M. Wuttig, Phys. Rev. B **43**, 8316 (1991).
[31] D. Veihland, J. F. Li, S. J. Jang, L. E. Cross, and M. Wuttig, Phys. Rev. B **46**, 8013 (2002).
[32] Q. Tan and D. Viehland, Phys. Rev. B **53**, 14103 (1996); X. Dai, Z. Xu, J. F. Li, and D. Viehland, J. Mater. Res. **11**, 618 (1996).
[33] G. A. Samara, J. Phys.: Condens. Matter **15**, R367 (2003).
[34] S. E. Park and T. R. Shrout, J. Appl. Phys. **82**, 1804 (1997).
[35] O. Noblanc, P. Gaucher, and G. Calvarin, J. Appl. Phys. **79**, 4291 (1996).
[36] G. A. Samara, E. L. Venturini, and V. H. Schmidt, Phys. Rev. B **63**, 184104 (2001).
[37] L. E. Cross, Ferroelectrics **76**, 241 (1987).
[38] J. Kreisel, P. Bouvier, M. Maglione, B. Dkhil, and A. Simon, Phys. Rev. B **69**, 092104 (2004).
[39] A. A. Bokov, M. Maglione, and Z. G. Ye, J. Phys.: Condens. Matter **19**, 092001 (2007).
[40] S. Ke, H. Fan, H. Huang, H. L. W. Chan, and S. Yu, J. Appl. Phys. **104**, 034108 (2008).
[41] M. Nagasawa, H. Kawaji, T. Tojo, and T. Atake, Phys. Rev. B **74**, 132101 (2006).
[42] S. Miao, J. Pokorny, U. M. Pasha, O. P. Thakur, D. C. Sinclair, and M. Reaney, J. Appl. Phys. **106**, 114111 (2009).
[43] C. Laulhé, F. Hippert, J. Kreisel, M. Maglione, A. Simon, J. L. Hazemann, and V. Nassif, Phys. Rev. B **74**, 014106 (2006).
[44] J. Petzelt, D. Nuzhnyy, V. Bovtun, M. Kempa, M. Savinov, S. Kamba, and J. Hlinka, Phase Transitions **88**, 320 (2015).
[45] J. Petzelt, D. Nuzhnyy, M. Savinov, V. Bovtun, M. Kempa, T. Ostapchuk, J. Hlinka, G. Canu, and V. Buscaglia, Ferroelectrics **469**, 14 (2014).
[46] S. Prosandeev, D. Wang, A. R. Akbarzadeh, and L. Bellaiche, J. Phys.: Condens. Matter **27**, 223202 (2015).
[47] R.-J. Carvajal, FULLPROF 2000 A Rietveld Refinement and Pattern Matching Analysis Program, Laboratories Leon Brillouin (CEA-CNRS), France.
[48] B. N. Rao and R. Ranjan, Phys. Rev. B **86**, 134103 (2012).
[49] K. V. Lalitha, A. N. Fitch, and R. Ranjan, Phys. Rev. B **87**, 064106 (2013).
[50] B. N. Rao, A. N. Fitch, and R. Ranjan, Phys. Rev. B **87**, 060102(R) (2013).
[51] A. A. Bokov, Y.-H. Bing, W. Chen, Z.-G. Ye, S. A. Bogatina, I. P. Raevski, S. I. Raevskaya, and E. V. Sahkar, Phys. Rev. B **68**, 052102 (2003).
[52] A. A. Bokov and Z.-G. Ye, Phys. Rev. B **65**, 144112 (2002).
[53] A. K. Kalyani, D. K. Khatua, B. Loukya, R. Datta, A. N. Fitch, A. Senyshyn, and R. Ranjan, Phys. Rev. B **91**, 104104 (2015).
[54] R. Garg, B. N. Rao, A. Senyshyn, P. S. R. Krishna, and R. Ranjan, Phys. Rev. B **88**, 014103 (2013).
[55] J. Y. Li, R. C. Rogan, E. Üstündag, and K. Bhattacharya, Nature Mater. **4**, 776 (2005).
[56] A. Pramanick, D. Damjanovic, J. E. Daniels, J. C. Nino, and J. L. Jones, J. Am. Ceram. Soc. **94**, 293 (2011).
[57] Y. M. Jin, Y. U. Wang, A. G. Khachaturyan, J. F. Li, and D. Viehland, J. Appl. Phys. **94**, 3629 (2003).
[58] J. Gao, D. Xue, Y. Wang, D. Wang, L. Zhang, H. Wu, S. Guo, H. Bao, W. Liu, S. Hou, G. Xiao, and X. Ren, Appl. Phys. Lett. **99**, 092901 (2011).
[59] M. Hinterstein, M. Hoelzel, J. Rouquette, J. Haines, J. Glaum, H. Kungl, and M. Hoffman, Acta Mater. **94**, 319 (2015).
[60] K.V. Lalitha, C. M. Fancher, J. L. Jones, and R. Ranjan, arXiv:1508.05734.
[61] N. Zhang, H. Yokota, A. M. Glazer, and P. A. Thomas, Acta. Crystallogr., Sect. B: Struct. Sci. **67**, 386 (2011).
[62] Ragini, R. Ranjan, S. K. Mishra, and D. Pandey, J. Appl. Phys. **92**, 3266 (2002).
[63] D. L. Corker, A. M. Glazer, R. W. Whatmore, A. Stallard, and F. A. Fauth, J. Phys.: Condens. Matter **10**, 6251 (1998).
[64] T. R. Welberry, D. J. Goossens, and M. J. Gutmann, Phys. Rev. B **74**, 224108 (2006).
[65] W. Ge, C. P. Devreugd, D. Phelan, Q. Zhang, M. Ahart, J. Li, H. Luo, L. A. Boatner, D. Viehland, and P. M. Gehring, Phys. Rev. B **88**, 174115 (2013).
[66] I. Grinberg, V. R. Cooper, and A. M. Rappe, Phys. Rev. B **69**, 144118 (2004).
[67] A. M. Glazer, P. A. Thomas, K. Z. Baba-Kishi, G. K. H. Pang, and C. W. Tai, Phys. Rev. B **70**, 184123 (2004).
[68] N. Zhang, H. Yokota, A. M. Glazer, Z. Ren, D. A. Keen, D. S. Keeble, P. A. Thomas, and Z.-G. Ye, Nat. Commun. **5**, 5231 (2014).
[69] M. Matsura, K. Hirota, P. M. Gehring, Z. G. Ye, W. Chen, and G. Shirane, Phys. Rev. B **74**, 144107 (2006).
[70] G. Xu, Z. Zhong, Y. Bing, Z.-G. Ye, and G. Shirane, Nature (London) **5**, 134 (2006).
[71] D. Nuzhnyy, J. Petzelt, M. Savinov, T. Ostapchuk, V. Bovtun, M. Kempa, J. Hlinka, V. Buscaglia, M. T. Buscaglia, and P. Nanni, Phys. Rev. B **86**, 014106 (2012).
[72] A. R. Akbarzadeh, S. Prosandeev, E. J. Walter, A. Al-Barakaty, and L. Belliache, Phys. Rev. Lett. **108**, 257601 (2012).
[73] D. Wang, J. Hlinka, A. A. Bokov, Z.-G. Ye, P. Ondrejkovic, J. Petzelt, and L. Bellaiche, Nat. Commun. **5**, 5100 (2014).